Exploring the Ability of Frozen-Density Embedding to Model Induced Circular Dichroism

Johannes Neugebauer*,† and Evert Jan Baerends*

Theoretical Chemistry, Vrije Universiteit Amsterdam, De Boelelaan 1083, 1081 HV Amsterdam, The Netherlands

Received: April 10, 2006; In Final Form: May 15, 2006

In this study, we present calculations of the circular dichroism (CD) spectra of complexes between achiral and chiral molecules. Nonzero rotational strengths for transitions of the nonchiral molecule are induced by interactions between the two molecules, which cause electronic and/or structural perturbations of the achiral molecule. We investigate if the chiral molecule (environment) can be represented only in terms of its frozen electron density, which is used to generate an effective embedding potential. The accuracy of these calculations is assessed in comparison to full supermolecular calculations. We can show that electronic effects arising from specific interactions between the two subsystems can reliably be modeled by the frozen-density representation of the chiral molecule. This is demonstrated for complexes of 2-benzoylbenzoic acid with (−)-(*R*)-amphetamine and for a nonchiral, artificial amino acid receptor system consisting of ferrocenecarboxylic acid bound to a crown ether, for which a complex with L-leucine is studied. Especially in the latter case, where multiple binding sites and interactions between receptor and target molecule exist, the frozen-density results compare very well with the full supermolecular calculation. We also study systems in which a cyclodextrin cavity serves as a chiral host system for a small, achiral molecule. Problems arise in that case because of the importance of excitonic couplings with excitations in the host system. The frozen-density embedding cannot describe such couplings but can only capture the direct effect of the host electron density on the electronic structure of the guest. If couplings play a role, frozen-density embedding can at best only partially describe the induced circular dichroism. To illustrate this problem, we finally construct a case in which excitonic coupling effects are much stronger than direct interactions of the subsystem densities. The frozen density embedding is then completely unsuitable.

1. Introduction

Induced circular dichroism (ICD) is the phenomenon that the circular dichroism (CD) spectrum of a mixture of two compounds differs from the sum of the spectra of the two individual compounds. Most attention has been paid to cases of ICD in which an achiral chromophore shows circular dichroism in the presence of a chiral partner, in particular when the latter alone does not show CD activity in the wavelength regime investigated in a certain experiment. In those cases, a CD signal can be observed when combining the two compounds while there is no signal for either of the individual compounds.

This effect is related to interactions between the achiral chromophore and the chiral partner in its surrounding. The most important examples are symmetric compounds in optically active solvents and complexes between chiral and achiral molecules. A special case of the latter are host−guest complexes with achiral guest molecules in chiral hosts. Two basic mechanisms causing ICD can be distinguished,[1] a structural perturbation of the achiral guest by the chiral partner, and an electronic perturbation of the guest due to the chiral environment. For the structural effects, a further classification can be made into (i) symmetric molecules that are inherently nonchiral, but for which a chiral, nonsymmetric structure is favored in the presence of the chiral environment, and (ii) molecules with inherently chiral structures, which are not optically active because of low barriers between the enantiomeric forms, but for which a chiral partner selectively stabilizes one enantiomeric form. The former molecules are nonchiral already in a static picture (e.g., benzene), whereas the latter are only nonchiral on average (or in a dynamic picture), as both enantiomeric forms will occur with equal probabilities (e.g., hydrogen peroxide).

Many systems showing ICD have been investigated experimentally. In particular the class of cyclodextrins has been studied in detail as a host system for many small, achiral molecules, for example, benzoylbenzoic acid,[2] different azi- and diaziadamantanes (see ref 1), 2,3-diazabicyclo[2.2.2]oct-2-ene and derivatives,[3,4] substituted benzenes,[5] *N*-bromophthalimide,[6] maleimide,[7] and naphthalene[8] and its derivatives,[9] as well as fluorenone and xanthone.[10] A more extensive overview over cyclodextrin inclusion compounds can be found in refs 11, 12. Tokura and co-workers investigated the induced circular dichroism and its solvent dependence in the 2-benzoylbenzoic acid-amphetamine system.[13,14] Another application of ICD is its use for chirality sensing, for example, for amino acids, as demonstrated in ref 15.

Computational studies on induced circular dichroism are often restricted to classical molecular mechanics (MM) approaches or semiempirical approaches, especially for the relatively large systems of cyclodextrin compounds.[7,10,16] In many cases, the intensity analyses for the CD spectra are based on the Kirkwood model of coupled oscillators[17] or, to be more precise, on the modified Kirkwood expression based on bond polarizabilities developed by Tinoco[18] (see, e.g., the work in refs 8, 10, 19,

* To whom correspondence should be addressed. E-mail: (J.N.) johannes.neugebauer@phys.chem.ethz.ch; (E.J.B.) baerends@chem.vu.nl.
† Present address: Laboratory of Physical Chemistry, ETH Zurich, Wolfgang-Pauli-Strasse 10, 8093 Zurich, Switzerland.

10.1021/jp0622280 CCC: $33.50
Published on Web 06/20/2006

and 20). Such investigations resulted in Harata's rule, which states that the ICD of a chromophore inside the cyclodextrin cavity will always be positive if its electric transition dipole moment is parallel to the principal axis of the cyclodextrin cavity,[1,8] and negative, if it is perpendicular. Additionally, Kodaka's rule states that the situation is reversed if the chromophore is located outside the cyclodextrin cavity.[21,22]

Because of the size of the host molecule, first-principles calculations of excitation energies and rotational strengths for these systems are rather demanding. Although TDDFT calculations may still be feasible for these systems, they suffer from spuriously low long-range inter- and intramolecular charge-transfer (CT) excitations. In particular for rather weakly bound systems, like the supramolecular complexes for which ICD is reported, many of such artificially low excitations occur. This problem is due to the well-known failure of the exchange-correlation kernel in ALDA-TDDFT.[23−25] In two recent papers,[26,27] we could show that this problem can be avoided by the frozen-density embedding (FDE) method, originally introduced by Wesolowski and Warshel,[28,29] and its time-dependent response generalization.[30] In this DFT-in-DFT embedding method, the effect of a medium on a chromophore is included by an effective embedding potential, which only depends on the charge density of the surrounding medium. Our papers addressed the problem of modeling the effect of a large solvent shell on the absorption spectrum of acetone[26] or an aminocoumarin dye.[27] In this work, we want to study the ability of FDE to capture the effect of induced circular dichroism by more complex surroundings, consisting of chiral partners in supramolecular aggregates or symmetry-breaking host systems. Since the response of the environment (the frozen system) is explicitly assumed to be negligible in the implementation of the frozen-density TDDFT scheme,[26,27,31] only those systems can be treated in which the circular dichroism is due to transitions in the embedded system. If transitions in both systems are important, it would still be possible to do two FDE calculations with either the one or the other system frozen, so that the contributions of the two molecules can be calculated separately. However, effects arising from a coupling of electronic transitions in the two systems cannot be described correctly by this type of frozen-density embedding. But it should be a valuable tool if the ICD can be described in terms of the perturbation of the guest's electronic structure by the host system's charge density.

After a short outline of the methodology in section 2, we analyze the results of FDE in calculations of the CD spectra of complexes between 2-benzoylbenzoic acid and (−)-(*R*)-amphetamine in section 3. As an example with a more complicated electronic structure, we present results for a ferrocenecarboxylic acid-crown ether conjugate with protonated L-leucine in section 4. The aim of these sections is to analyze the advantages and shortcomings of FDE, in particular in comparison to TDDFT calculations for the full complex, while a direct comparison to experiment would require a much more extensive survey of possible low-energy structures. Section 5 deals with phenol as a guest in a cyclodextrin host molecule. The inability of frozen-density embedding to describe excitonic couplings to the frozen-density region, which is a consequence of its restriction to the orbital space of the embedded system, is illustrated for the benzaldehyde dimer in section 6. Finally, conclusions are drawn in section 7.

2. Methodology

The basic idea of the orbital-free embedding method, which is explained in more detail elsewhere,[28,29] is the partitioning of the electron density of the total system to be described into the density of an embedded subsystem (ρ_I) and the density of its microscopic environment (ρ_{II}). This environment is described only in terms of the density ρ_{II}, and the nuclear charges $Z_{A_{II}}$ at the positions $\mathbf{R}_{A_{II}}$ in the environmental system. The aim of the calculation is then to find the total density $\rho_{total} = \rho_I + \rho_{II}$ of the system which minimizes the total energy $E[\rho_{total}]$ with the constraint that ρ_{II} is kept frozen. From this requirement we can derive Kohn−Sham-like one-electron equations for orbitals of the embedded system (system I), which define the optimum density ρ_I. They contain the same effective potential as present in conventional Kohn−Sham calculations plus an effective embedding potential (at position $\mathbf{r}$) of the form

$$V_{emb}^{eff}(\mathbf{r})[\rho_I,\rho_{II}] = \sum_{A_{II}} -\frac{Z_{A_{II}}}{|\mathbf{r}-\mathbf{R}_{A_{II}}|} + \int \frac{\rho_{II}(\mathbf{r}')}{|\mathbf{r}'-\mathbf{r}|}\,d\mathbf{r}' + \left.\frac{\delta E_{xc}[\rho]}{\delta\rho}\right|_{\rho=\rho_I+\rho_{II}} - \left.\frac{\delta E_{xc}[\rho]}{\delta\rho}\right|_{\rho=\rho_I} + \left.\frac{\delta T_s[\rho]}{\delta\rho}\right|_{\rho=\rho_I+\rho_{II}} - \left.\frac{\delta T_s[\rho]}{\delta\rho}\right|_{\rho=\rho_I} \quad (1)$$

where the exchange-correlation ($E_{xc}[\rho]$) and kinetic-energy ($T_s[\rho]$) functionals are defined in the Kohn−Sham formulation of density functional theory (DFT). The kinetic energy part of the potential may also be written as the functional derivative $\delta T_s^{nadd}[\rho_I,\rho_{II}]/\delta\rho_I$ of the nonadditive kinetic energy functional

$$T_s^{nadd}[\rho_I,\rho_{II}] = T_s[\rho_I+\rho_{II}] - T_s[\rho_I] - T_s[\rho_{II}] \quad (2)$$

We use the gradient-dependent approximation for $T_s^{nadd}[\rho_I,\rho_{II}]$[29] denoted as PW91k in ref 26. Since we employ the orbital-dependent "statistical averaging of (model) orbital potentials" (SAOP) potential[32−34] for the nonfrozen system, we approximate the exchange-correlation component of the effective embedding potential by the Becke−Perdew−Wang (BPW91) exchange-correlation functional.[35,36] Although this introduces a slight inconsistency in the treatment of frozen and nonfrozen subsystem, the use of different exchange-correlation potentials for different subsystems is, from a pragmatic point of view, an advantage, as a more sophisticated potential with correct asymptotic behavior can be applied for the embedded system. It turned out that the combination of these potentials works quite well for FDE calculations of absorption spectra.[26,27] Also for (induced) dipole moments and polarizabilities of van der Waals complexes, different combinations of exchange-correlation potentials have been tested.[37]

A time-dependent linear response generalization of this embedding scheme was derived in ref 30. Under the assumption that the response to an external electromagnetic field in resonance with an electronic transition of the embedded molecule is localized to system I, that is, that the response of the environment (system II) can be neglected, this leads, in addition to the kernel within the adiabatic local density approximation (ALDA) in conventional TDDFT, to an effective embedding kernel (see the Supporting Information to ref 31)

$$f_{xc}^{emb}(r,r') = \left.\frac{\delta^2 E_{xc}[\rho]}{\delta\rho(\mathbf{r})\,\delta\rho(\mathbf{r}')}\right|_{\rho=\rho_I+\rho_{II}} - \left.\frac{\delta^2 E_{xc}[\rho]}{\delta\rho(\mathbf{r})\,\delta\rho(\mathbf{r}')}\right|_{\rho=\rho_I} + \frac{\delta^2 T_s^{nadd}[\rho_I,\rho_{II}]}{\delta\rho_I(\mathbf{r})\,\delta\rho_I(\mathbf{r}')} \quad (3)$$

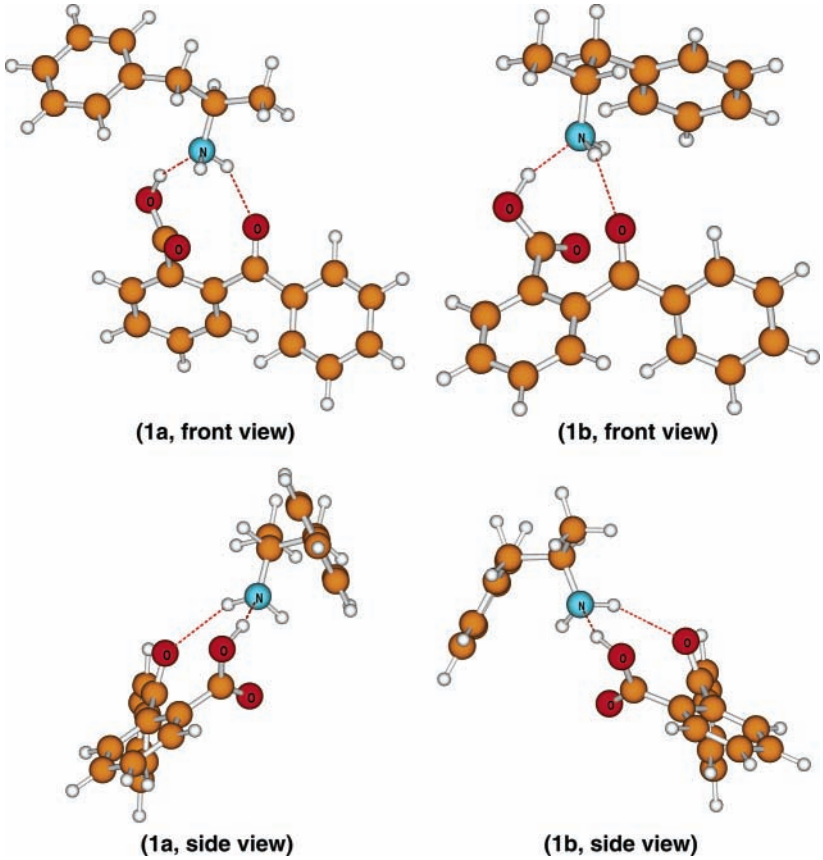

Figure 1. Optimized (BP86/TZP) structures of the benzoylbenzoic acid−(−)-(*R*)-amphetamine complex. The structure of benzoylbenzoic acid in complex **1b** is the (reoptimized) mirror image of that in complex **1a** (the mirror plane is approximately the plane of the benzoyl group; see side views on lower panel). Note that the amphetamine rotated around the C−N bond during reoptimization. The energy difference between the two complexes is 0.6 kJ/mol.

which now also contains a kinetic energy contribution. This contribution is, for consistency with the ALDA-kernel, approximated by using the (local density) Thomas-Fermi functional

$$T_s^{TF} = C_{TF} \int \rho^{5/3} d\mathbf{r} \tag{4}$$

This means that the additional term depending on the solvent response function in the exact formulation in ref 30 is assumed to be negligible. Alternatively, we assume that the whole response can be described in terms of a change in the density ρ_I. This assumption turned out to work well in the case of DNA base pairs[31] and solvated acetone,[26] but led to a slight underestimation of solvent shifts for the aminocoumarin dye C151,[27] which could be corrected by including a small number of solvent molecules in the embedded region.

The KSCED equations would, under the assumptions mentioned above, lead to the exact ground-state density ρ_{total} if the exact exchange-correlation and kinetic energy functionals would be known. In practical applications, however, it sometimes turns out that the density ρ_I is not flexible enough to arrive at the optimum total density. In those cases, so-called freeze-and-thaw cycles can be used,[29] in which the role of the systems I and II is reversed in order to relax ρ_{II} with respect to ρ_I. If this procedure is carried out iteratively, the effect is a full minimization of the energy as a bifunctional of the densities ρ_I and ρ_{II}. In that sense, the ground-state frozen-density embedding calculations are not an approximation, but an alternative to conventional Kohn−Sham calculations.

For excitation energies it turned out that one freeze-and-thaw cycle is typically sufficient to converge the excitation energies within less than 0.01 eV, and even the results without relaxation of ρ_{II} are reasonable.[26,27,31] A limitation arises from the fact that couplings between electronic transitions in subsystems I and II cannot be described by FDE: Electronic transitions in subsystem II, or inter-subsystem transitions, are excluded, since the orbital-space is restricted to subsystem I. Therefore, FDE is not applicable if coupled excitations for chromophores in different subsystems determine the spectroscopic properties.

In the following, we are going to test whether this limitation plays a role in describing the phenomenon of induced circular dichroism. All calculations are carried out using the program package ADF.[38,39] We employ the Becke-Perdew functional, dubbed BP86,[35,40] in combination with the TZP basis set from the ADF basis set library[38] for structure optimizations. For subsequent TDDFT calculations with the SAOP potential,[32−34] we use the implementation of rotational strengths[41−43] in the ADF RESPONSE module[44] together with the frozen-density embedding approach. In the spectra plots, all vertical excitations are represented as Gaussian curves with a half-width of 0.4 eV. Graphics of the molecular structures were generated with the programs MOLDEN[45] and VMD.[46]

3. Benzoylbenzoic Acid−Amphetamine

The first compound studied here is a hydrogen-bonded complex between the nonchiral 2-benzoylbenzoic acid and (−)-(*R*)-amphetamine. The optimized structure of this complex is shown in Figure 1. This system has experimentally been studied in detail by Tokura and co-workers.[2,13] They found strong evidence for the formation of a 1:1 complex between the two molecules in solution. From the vibrational frequencies and the solvent dependence of the ICD signal, they concluded that the

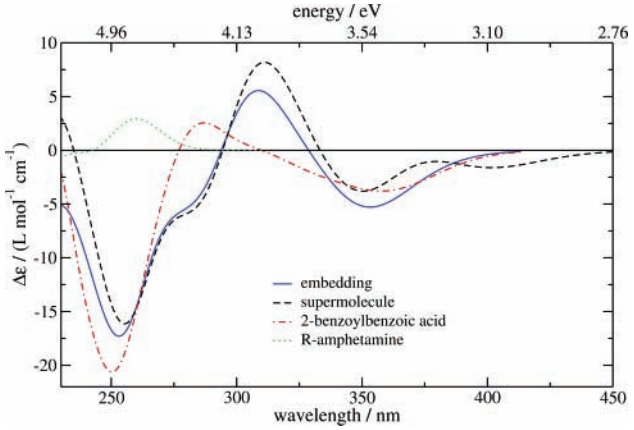

Figure 2. CD spectra of the 2-benzoylbenzoic acid−(−)-(*R*)-amphetamine complex **1a** in Figure 1. Shown are spectra from an embedding calculation in which the amphetamine was represented by its frozen density (solid line), a supermolecular calculation (dashed line), as well as the spectra of isolated benzoylbenzoic acid (dashed−dotted line) and (−)-(*R*)-amphetamine (dotted line) in the structures they assume in complex **1a**.

complex was formed by the deprotonated acid and the protonated amphetamine.[13] The ICD signal was found to be weaker in polar solvents, which favor the separation of the ion pair. Our optimization of the isolated complex did not lead to an ion pair structure, although the hydrogen bond between the amino-N and the proton of the carboxyl-group is relatively short (1.7 Å in structure **1a**). Since the goal of this study is an assessment of frozen-density embedding for modeling the ICD effect, we refrain from a detailed discussion of this structural feature. A more detailed study of structural and vibrational properties of this complex, including the vibrational circular dichroism spectra, which can also shed more light on the type of binding between the two molecules, is under way.[47]

In this system, (−)-(*R*)-amphetamine acts as the chiral part that shall be described in terms of its frozen density. The isolated amphetamine in the structure of complex **1a** shows only very weak CD intensity in the wavelength range investigated in this work, and no transition for this molecule is observed below 4.75 eV. Furthermore, the lowest excitations of (−)-(*R*)-amphetamine are shifted to higher energies (>5 eV) in complex **1a**, so that its contribution to the total CD spectrum is not relevant for our purposes and consequently will not be discussed here. Benzoylbenzoic acid is the nonchiral part in this system, but it is nonchiral only in a dynamical sense (see section 1). In its structure in **1a** it is chiral, and it has a nonzero CD spectrum as shown in Figure 2. A broad negative CD band from several overlapping transitions can be observed at 360 nm, and a weak positive band occurs at 287 nm, followed by a stronger negative band at 250 nm.

To see if there is an induced circular dichroism in complex **1a** we calculated the CD spectrum of this complex in a supermolecular calculation. The resulting spectrum is included in Figure 2. The CD spectrum of the isolated 2-benzoylbenzoic acid in the structure of complex **1a** differs significantly from the CD spectrum of the whole complex (as obtained in the supermolecular calculation). First, we observe a weak negative band at 402 nm. However, this is a spurious transition in the supermolecular calculation, since it represents partial charge-transfer between the two molecules. ALDA-TDDFT does not describe such transitions correctly, yielding typically much too low excitation energies. Besides this feature, the most important differences are a strong positive band at 312 nm and a shoulder (at 282 nm) to the strong negative band at 256 nm, which is shifted a bit compared to the isolated 2-benzoylbenzoic acid and shows slightly lower intensity. This comparison shows that there is an important electronic contribution because of the effect arising from the amphetamine on the 2-benzoylbenzoic acid.

TABLE 1: Excitation Energies E_{Ex} (SAOP/TZP; in Units of eV) and Rotational Strengths R (in cgs Units of 10^{-40} esu^2 cm^2) for Complex 1a in Figure 1[a]

	supermolecule		embedding		isolated	
no.	E_{ex}	R	E_{ex}	R	E_{ex}	R
1	2.87	0.02				
2	3.04	−0.48				
3	3.18	−9.46	3.28	−0.84	3.66	−2.54
4	3.34	12.54				
5	3.51	−16.76	3.52	−14.79	3.42	−9.36
6	3.86	6.51	3.86	8.60	4.04	4.45
7	3.92	−11.71	3.91	−13.92	3.82	−3.22
8	4.00	27.88	4.03	21.55	4.30	2.00
9	4.13	−0.15				
10	4.21	−0.03				
11	4.30	0.32				
12	4.34	−13.49	4.33	−10.31	4.16	−5.60
13	4.37	−0.26				
14	4.41	0.27	4.54	1.52	5.09	−1.45
15	4.45	0.01				
16	4.49	5.37	4.56	−2.30	4.57	−2.05
17	4.51	−5.59				
18	4.60	−0.14	4.52	−2.47	4.35	7.62
19	4.62	−0.05				
20	4.65	0.41				
21	4.72	−6.60	4.74	−3.39	4.88	−3.74
22	4.73	0.42	4.78	−3.85	4.84	−1.08
23	4.84	−20.80	4.87	−18.46	4.95	−22.98

[a] For comparison, also the results for the isolated benzoylbenzoic acid in the structure of complex **1a** are given.

To answer the question whether this effect can be modeled in terms of an effective embedding potential, we carried out a calculation with a frozen-density representation of the chiral amphetamine molecule. Two freeze-and-thaw cycles were used in the embedding calculation, but the differences with respect to the results obtained with one freeze-and-thaw cycle are negligible. Therefore, only one freeze-and-thaw cycle is used in all the other examples studied here if not explicitly stated otherwise. The resulting CD spectrum is shown in Figure 2. The electronic contribution is very nicely reproduced by the FDE calculation, in which the amphetamine was treated as the frozen system. We observe a negative band at 353 nm, a positive band at 309 nm, and a shoulder at 281 nm to the strong negative band, which has its maximum at 254 nm. Although the rotational strengths for the bands at 353 and 309 nm differ a bit from the corresponding supermolecular values, the general agreement between the two curves is very nice. The only feature which is missing in the frozen-density calculation is the low-intensity band at 402 nm. This is a transition of partial charge-transfer type between the two molecules, which is not reproduced correctly by ALDA-TDDFT (see section 5), and which cannot, by construction of the method,− be obtained in FDE calculations.

While the spectra shown in Figure 2 are a superposition of all excitations, we report the individual excitation energies and rotational strengths in Table 1. That table shows data for the isolated 2-benzoylbenzoic acid, the 2-benzoylbenzoic acid with the effective embedding potential of the (−)-(*R*)-amphetamine, and the complex of the two molecules ("supermolecule"). Corresponding excitations were found by mapping the excitations of the supermolecule on those excitations of the embedded or isolated molecule, for which the transition densities have the largest overlap (see ref 26).

TABLE 2: Excitation Energies E_{Ex} and Orbital Energy Differences $\Delta\epsilon^{orb}$ for the Most Important Orbital Pair in Those Excitations in Table 1 for Which No Corresponding Excitation Exists in the Embedding Calculation (SAOP/TZP; in Units of eV)

no.	E_{ex}	$\Delta\epsilon^{orb}$
1	2.87	2.87
2	3.04	3.04
4	3.34	3.30
9	4.13	4.13
10	4.21	4.21
11	4.30	4.30
13	4.37	4.37
15	4.45	4.45
17	4.51	4.41
19	4.62	4.62
20	4.65	4.63

It can be observed that there are some excitations for which no corresponding transitions can be found in the embedding or isolated calculation for 2-benzoylbenzoic acid. These are charge-transfer excitations from one of the two molecules to the other. For charge-transfer excitations, the XC-kernel in ALDA-TDDFT calculations completely fails: It yields a zero contribution, and the excitation energies reduce to the orbital energy differences of the orbitals involved, which is completely wrong. As can be recognized from Table 2, for almost all of these excitations missing in the embedded calculation, the orbital energy difference and the excitation energy are practically identical, which is a strong hint on their CT nature. Further characteristics of CT excitations are their low transition moments and rotational strenghts, which holds for all of these additional excitations except the ones at 3.34 and 4.51 eV, which also show the largest deviations from the orbital energy differences for the excitation energies in Table 2. Indeed, we find a mixed character of CT and intramolecular valence transitions for these two excitations. The rest of all these supermolecule CT excitations in Table 2 can be regarded as artifacts of the ALDA-TDDFT method, with much too low energies.

For the transitions which occur in both the supermolecular and the embedding calculation, the excitation energies typically agree very nicely within 0.03 eV, even for excitations that shift by up to 0.3 eV compared to the isolated calculation. For excitations which do exhibit differences between embedded and supermolecular calculation, the differences are still small compared to the shift with respect to the isolated 2-benzoylbenzoic acid. For example, the lowest singlet excitation in the isolated molecule shifts from 3.66 to 3.28 eV (embedding) or 3.18 eV (supermolecule), and the excitation at 5.09 eV in the isolated molecule shifts to 4.54 eV (embedding) or 4.41 eV (supermolecule). There is no excitation for which the embedding predicts a wrong direction of the shift. Also the rotational strengths are quite similar, which leads to the very good overall agreement of the spectra. There is one exception for the rotational strengths: The excitation at 3.18 eV in the supermolecular calculation has a large negative rotational strength, while the embedding calculation predicts a transition at 3.28 eV with a small negative rotational strength. In the supermolecular calculation, there is another transition with large positive rotational strength at 3.34 eV, which also has a reasonable transition density overlap with the excitation at 3.28 eV in the embedding calculation. This excitation at 3.34 eV is as noted earlier a spurious CT transition (cf. Table 2), but being accidentally close to another excitation, it distorts the rotational strengths of the two transitions, picking up much to high rotational strength itself and leaving a much too high (negative) rotational strength for the excitation at 3.18 eV. The net effect

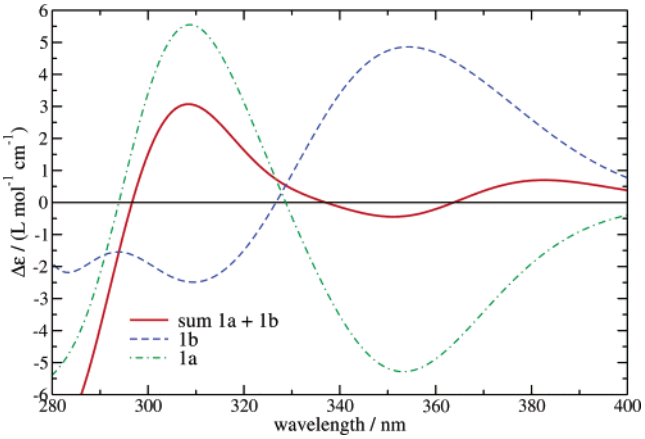

Figure 3. CD spectra of the benzoylbenzoic acid−(−)-(*R*)-amphetamine complexes **1a** (dotted line) and **1b** (dashed line) in Figure 1 as well as the sum of these two spectra (solid line).

in the spectra is quite similar: both in the supermolecular and in the embedding calculation, the total CD signal in that energy range is quite small. Also for the excitations at 4.49, 4.51, and 4.60 eV in the supermolecular calculation, we observe a rather strong mixing between different orbital transitions, one of which is of CT type, leading to a cancellation of the rotational strengths.

From this example, it can be concluded that frozen-density embedding is very well suited to reproduce the change in the CD spectrum due to the interactions with the chiral, hydrogen-bonded partner molecule.

Although it is not the aim of this work to provide a detailed comparison with experiment, we would like to outline which steps would be necessary to simulate the behavior of the real system in solution. Up to now, we only looked at one particular optimized structure, although several other local minima might be energetically accessible and therefore important in solution. In particular, it could be argued that we started from an already chiral structure for the benzoylbenzoic acid, while its mirror image will occur with the same probability in solution in absence of a chiral partner. Therefore, the next step in the analysis of this system is to reoptimize the complex, but starting from the conformer of benzoylbenzoic acid that is the mirror image of the structure in **1a**. We carried out such an optimization, which resulted in structure **1b**. From the lower panel in Figure 1 it can be seen that indeed the benzoylbenzoic acid moiety is just mirrored with respect to the structure in **1a**. During reoptimization, the (−)-(*R*)-amphetamine rotated around the C−N bond. The energy difference between the two conformers **1a** and **1b** is only 0.6 kJ/mol, so that both forms will exist in almost identical amounts in solution, and they would equally contribute to the total CD spectrum. Therefore, we performed another FDE calculation on structure **1b**, and the resulting CD spectrum is shown in Figure 3. That figure also contains the spectrum of **1a** as well as the sum of the two spectra in the wavelength range which was investigated in the experiment.[13] It can be seen that the CD intensity for wavelengths between 340 and 400 nm more or less disappears because of the different signs in the CD bands for the two conformers. Between 300 and 320 nm, however, a net positive CD signal can be observed, because the negative band of structure **1b** is much less intense than the positive band of **1a**. This positive CD band with a maximum at 309 nm arises from $\pi \rightarrow \pi^*$ transitions in **1a** and **1b**.

To really mimic the situation in solution, it would be necessary to investigate many other low-energy structures and to sample their contribution to the total CD spectrum. Neverthe-

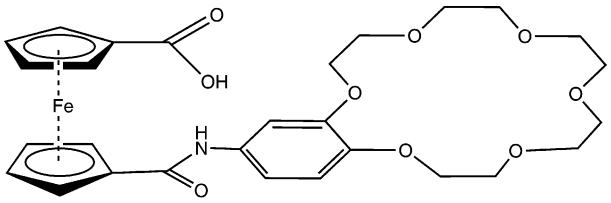

2

Figure 4. Lewis structure of the ferrocenecarboxylic acid-crown ether conjugate **2**.

less, it is gratifying to note that also in the experiment a positive CD band with a maximum at $\lambda_{max} \approx$ 318 to 326 nm (depending on the solvent) is the characteristic feature in the CD spectrum of 2-benzoylbenzoic acid induced by (−)-(*R*)-amphetamine.[13]

4. Complex of Ferrocenecarboxylic Acid-Crown Ether Conjugate and Leucine

Our second test system is a complex between the ferrocenecarboxylic acid-crown ether conjugate **2**, which is shown in Figure 4, and the protonated amino acid L-leucine. Like benzoylbenzoic acid in the first example, compound **2** is nonchiral only in a dynamical sense; that is, stable structures of **2** are chiral, but the system is flexible enough so that the enantiomeric forms are accessible in solution. Compound **2** contains multiple binding sites for amino acids: The carboxylic acid group can form two-point hydrogen bonds to the $-CO_2H$ group group of an amino acid, and the crown ether moiety can bind (protonated) amino groups. Therefore, the system can be seen as an artificial amino acid receptor, and was shown to enable efficient extraction of protonated amino acids from aqueous solution.[15] This system has been applied in chirality sensing studies, since α-amino acids induce a nonzero circular dichroism in complexes with the nonchiral **2**. In this way, **2** allows discrimination between the optical antipodes of α-amino acids, for example, L- and D-leucine,[15] which by themselves do not show CD activity for wavelengths > 250 nm. The optimized (BP86/TZP) structure (**3a**) of this complex is shown in Figure 5.

Again, we treat the chiral molecule, that is, L-leucine, as the frozen part in our calculation, to test whether the effect of the chirality-inducing subsystem can be reproduced by frozen-density embedding. This application may seem to be somewhat unusual, since the "environmental system" in this case is smaller than the actual embedded system, and from a computational point of view also the full supermolecular calculation is feasible. But FDE not only reduces the computational cost, it also opens up the way to a simpler interpretation of the induced circular dichroism signal in terms of an effective chiral perturbation in the potential.

The lowest singlet excitation of L-leucine in a calculation on its structure in **3a** was found at 5.28 eV (235 nm). Therefore, there will be no direct contribution of this amino acid to the spectrum of the complex in the wavelength range investigated here. Since compound **2** in structure **3a** is chiral, we first calculated the CD spectrum of isolated **2**, which is shown in Figure 6. The lowest excitations of **2** all involve orbital transitions from Fe *d*-type orbitals to π^* type orbitals of the substituted cyclopentadienyl (Cp) ligands, which also have partly Fe *d* contributions. At somewhat higher energies, these transitions are augmented with $\pi \rightarrow \pi^*$ excitations of the benzene moiety and $n(O) \rightarrow \pi^*(Cp)$ excitations. Most of the bands observed for **2** in this structure show a rather low intensity, for example, the negative bands with maxima at 433 nm and 528 nm. However, there are also two strong negative peaks at 333 and 285 nm.

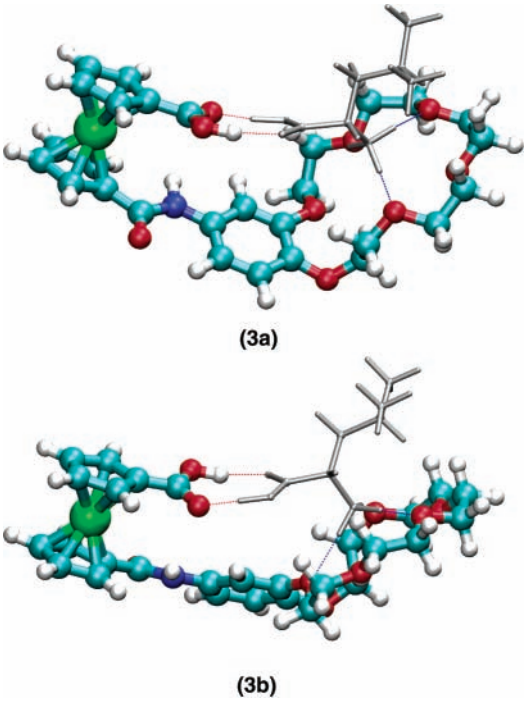

Figure 5. Optimized (BP86/TZP) structures of the complex between the ferrocenecarboxylic acid-crown ether conjugate (colored, ball-and-stick) and protonated L-leucine (grey, sticks only). The total charge of the complex is +1. Complex **3b** is a reoptimized complex starting from L-leucine and compound **2** in the mirror image structure of its optimum structure in complex **3a**. Structure **3a** is 1.2 kJ/mol lower in energy than structure **3b**.

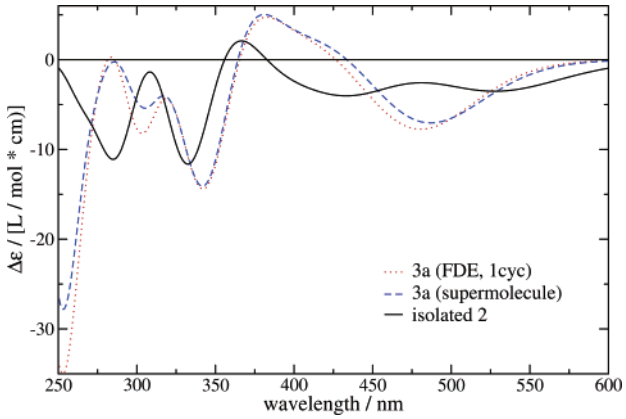

Figure 6. CD spectra of the complex **3a** in Figure 5. Shown are spectra from a calculation in which L-leucine was represented by its frozen electron density (dotted line), a supermolecular calculation (dashed line), as well as the spectrum of isolated compound **2** in the structure of complex **3a** (solid line).

When we include L-leucine into the calculation by performing a supermolecular calculation on complex **3a**, we observe a strong electronic effect that completely changes the CD spectrum: A stronger negative band appears at 488 nm and a positive band at 380 nm with a shoulder at 419 nm. The strong negative peak is now shifted to 342 nm and has even gained intensity. Another negative band can be seen at 304 nm. On the short-wavelength end of this spectrum, we see a very strong negative band centered at 253 nm. These features are very well reproduced if we use frozen-density embedding. There is only a slight disagreement in the position of the maximum of the first (negative) band (481vs 488 nm in the supermolecular

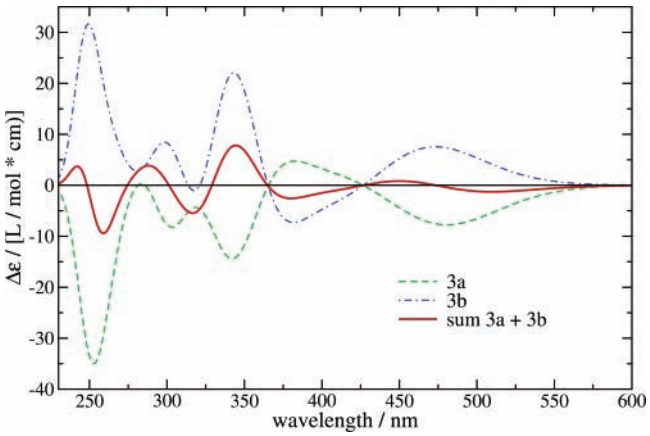

Figure 7. CD spectra of the complexes **3a** (dashed line) and **3b** (dashed−dotted line) in Figure 5 as well as the sum of these two spectra (solid line).

calculation), and the negative bands at 304 and 253 nm gain some intensity in the embedding calculation. This shows that even in situations of complex interactions between a receptor-like molecule and its substrate, the effect on the circular dichroism spectrum can reliably be modeled by FDE.

Also in this case, an extensive sampling over important conformations of this complex in solution would be necessary for a reliable comparison to experiment. Such a sampling would be even more demanding than for the system of 2-benzoylbenzoic acid and (−)-*R*-amphetamine. This is due to the fact that compound **2** is very flexible, and many low-energy configurations might be found. Again, a first step into this direction can be taken by optimizing the structure of the complex in which the mirror image of compound **2** in its structure in complex **3a** is employed, together with protonated L-leucine. We carried out such an optimization, which resulted in structure **3b** in Figure 5. The spectra of both complexes from frozen-density calculations and their sum are shown in Figure 7.

Unfortunately, it is very difficult to draw even qualitative conclusions from this sum spectrum in comparison to the experimental spectrum in ref 15. The experimental spectrum for the complex formed with protonated L-leucine shows a weak negative CD band at 310 nm, a positive CD band at 290 nm, and a broad negative CD band at about 255 nm. This spectral feature, denoted as a W-shaped band, is followed by a more intense negative band at ca. 225 nm, that is, at the short-wavelength end of the spectrum. Taking the sum of the spectra of complexes **3a** and **3b**, we can reproduce the cancellation of positive and negative CD signals in the wavelength regime from 365 to 600 nm. Moreover, the superimposed spectra indeed lead to a W-shaped spectral feature with a positive band at 288 nm, and two negative peaks at 317 and 259 nm. But there are also parts of the spectrum that do not match the experiment: There is a positive CD band at 344 nm, for which there is no experimental counterpart, and the strong negative band at ca. 225 nm is not observed.

We should take care not to over-interpret these results: At first glance, the spectra of **3a** and **3b** look rather symmetrical to the zero-line. The sum of the two spectra will thus depend very strongly on the exact positions and rotational strengths of the individual transitions, and the typical errors in TDDFT excitation energies might already be too large to quantitatively reproduce the experimental pattern. Second, there are several overlapping bands, and already the type of broadening applied in the simulated spectra may change the overall shape of the spectrum considerably[48] (here, again a uniform broadening of 0.4 eV was applied to all vertical transitions). As a further complication, many more conformers of this complex may play a role in solution, as the system is highly flexible (at least in the crown-ether moiety). These structures will occur in solution with different probabilities, so that a (Boltzmann-) weighted sum of the spectra would have to be taken instead of the unweighted sum used here. We can, however, clearly conclude that our calculations strongly support the possibility of an alternating sequence of positive and negative CD signals in the wavelength regime between 250 and 350 nm by electronic transitions of the ferrocene function.

To cover the full structural effect, it would be necessary to sample many structures of this molecule in solution, for example, from a CPMD simulation. In that case, the present FDE technique can become practically very important, since the solvent molecules could also be included efficiently into the frozen environmental density.

5. Cyclodextrins

As mentioned in the Introduction, cyclodextrin inclusion compounds are subject to extensive studies on induced circular dichroism.[1] One example of a nonchiral compound as a guest in a cyclodextrin cavity is phenol in β-cyclodextrin, which is composed of seven glucose units. It has been reported that the sign of the circular dichroism depends on the orientation of the phenol molecule with respect to the axis of the cyclodextrin cavity.[19] From the experimental sign of a particular electronic transition, the orientation of the guest molecule in the cavity can be estimated.

Phenol as a guest molecule in its optimized conformation is nonchiral. Interactions with the chiral host may lead to a distortion of its geometry, so that a structural effect due to the host molecule induces circular dichroism. Here, we want to concentrate on possible electronic effects causing ICD and their dependence on the orientation of the phenol molecule inside the cavity. Therefore, we take an optimized (BP86/TZP) structure of an isolated phenol, which is placed inside the cavity of an optimized (BP86/TZP) conformation of β-cyclodextrin. The center-of-mass of phenol was placed in the center of the cyclodextrin cavity. The initial orientation, in which the C−O bond of phenol is in the plane of the cyclodextrin ring, is shown in Figure 8, as well as a 90° rotated one, where the C−O bond is perpendicular to the ring.

For the isolated planar phenol molecule, the electric transition dipole moments can be either in-plane (irrep A') or perpendicular to the plane (irrep A''). According to Harata's rule, A' excitations should show a change in the sign of the CD signal when the molecule is rotated by 90° (in the way shown in Figure 8), as the transition moment is in the cyclodextrin plane for certain orientations, and perpendicular to it for orientations rotated by 90° with respect to the former ones. For the transition under study here, that is, the lowest singlet ($n \rightarrow \pi^*$) excitation of phenol, the direction of the electric transition dipole moment is in the molecular plane, approximately perpendicular to the C−O bond (see Figure 9).

Harata's rule was derived from the empirical Kirkwood-Tinoco model, which treats the interactions between excitations in host and guest system as a dipole−dipole coupling between transition dipole moments. The transitions in the host system are approximated in this case as transitions of individual groups or bonds j. It has been noted[21] that the most important term determining the sign of the rotational strength R_i for a given transition i in the guest molecule is the geometrical factor $(GF)_j$ in the Tinoco expression,[18] which is usually defined as[8,19]

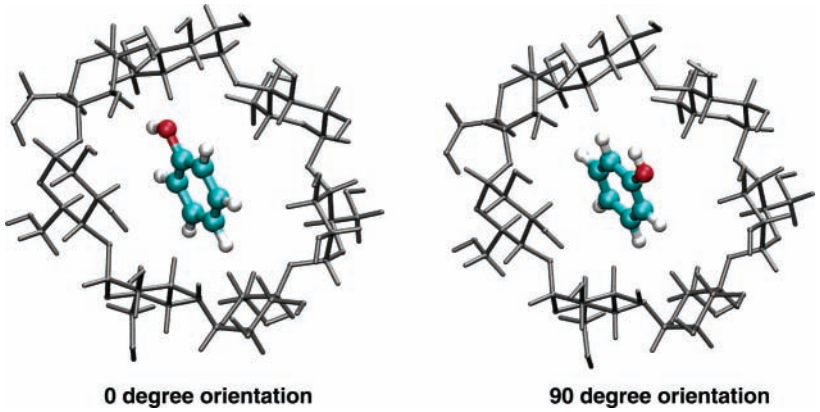

Figure 8. Structure of the host−guest complex **4** between phenol and β-cyclodextrin: left, 0° orientation; right, 90° orientation.

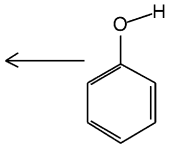

Figure 9. Direction of the electric transition dipole moment for the lowest singlet excitation of phenol. The transition dipole moment is located in the molecular plane.

$$(\mathrm{GF})_j = \frac{1}{r_{ij}^{\,3}}\left[\mathbf{e}_i\cdot\mathbf{e}_j - \frac{3(\mathbf{e}_i\mathbf{r}_{ij})(\mathbf{e}_j\mathbf{r}_{ij})}{r_{ij}^{\,2}}\right](\mathbf{e}_i \times \mathbf{e}_j)\cdot\mathbf{r}_{ij} \qquad (5)$$

In the above equation, $\mathbf{e}_i$ is the unit vector in the direction of the electric dipole transition moment of the guest molecule, $\mathbf{e}_j$ is the unit vector in the direction of the bond j, and $\mathbf{r}_{ij}$ is the vector between the two transition dipoles, which is assumed to be the vector from the center of the guest molecule to the center of bond j. Since $(\mathrm{GF})_j$ yields only the contribution of bond j, it is necessary to sum over all bond contributions to get the rotational strengths. The sum is a weighted sum in which bond polarizabilities parallel and perpendicular to the bond as well as an average wavenumber of the electronic transitions in that group enter as empirical parameters.[8,19]

Although we do not want to perform a detailed analysis of the performance of the Kirkwood-Tinoco model for our test case, it is interesting to see if qualitatively the behavior predicted by Harata's rule can be observed in our particular snapshot since eq 7 depends on the position and orientations of the bonds in the host system. To this end, we carried out a very simple analysis by performing an unweighted summation of the geometrical factors for all bonds. This was repeated for different orientations of the phenol molecule in the host cavity (the 0° and 90° orientations are shown in Figure 8). Such an approach corresponds to a very naive approximation within the Kirkwood-Tinoco model, namely, that the bond specific parameters are identical for all bonds. We only followed the common practice to neglect the effect of C−H bonds, which are usually assumed to have an isotropic bond polarizability that does not contribute to the total rotational strength. Tests indicated, however, that including the C−H bonds leads to the same qualitative behavior. For a more detailed analysis of phenol in β-cyclodextrin described by the Kirkwood-Tinoco model, we refer to ref 19.

The sum of the $(\mathrm{GF})_j$ for different angles of the C−O bond with respect to the plane in which the cyclodextrin molecule is located is shown in Figure 10. The data were obtained by using the transition dipole moment obtained for isolated phenol in each of these orientations. Since we are only interested in a qualitative behavior, the curve was scaled to match the results

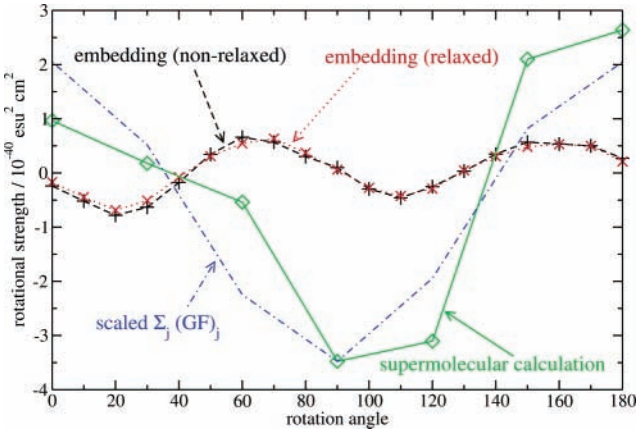

Figure 10. Rotational strength of the lowest singlet transition of the host−guest complex **4** between phenol and β-cyclodextrin with varying orientation of phenol inside the cavity. The 0 and 90° orientations are depicted in Figure 8. Shown are results from supermolecular calculations (SAOP/TZP/DZP), employing a simple CT-correction scheme[49], and from FDE calculations (SACP/TZP/CRP), in which the cyclodextrin was treated as the frozen system (either relaxed or nonrelaxed). For qualitative comparison, we also show (scaled) sums of the geometrical factors $(\mathrm{GF})_j$ for a given structure, which determine the rotational strength in the Kirkwood-Tinoco model.

of a supermolecular TDDFT calculation for the axial orientation (90°). Indeed, the qualitative behavior agrees with the calculations in ref 19; that is, we get positive values for equatorial orientations (0° and 180°) while the rotational strength is negative for the axial orientation of phenol (90°, corresponding to an equatorial orientation of the electric transition dipole moment). We also note that both our simple analysis and the empirical calculations in ref 19 lead to a behavior of the CD intensity that is symmetric with respect to the axial orientation (note that in Figure 11 of that reference, the angle is measured for the electric transition dipole moment, not for the C−O bond).

To investigate whether these results are confirmed by first principles methods, we performed full supermolecular TDDFT calculations on this system for certain orientations. In these calculations, we used the SAOP potential in combination with a TZP basis set for phenol and a DZP basis set for β-cyclodextrin. Since the system is quite extended (160 atoms), there is a severe problem with spuriously low charge-transfer excitations. To remove these unphysically low excitations, we applied the simple CT correction scheme originally proposed in ref 25. In ref 49 we could show that this correction scheme can efficiently be implemented and is particularly well suited for extended systems composed of weakly interacting subunits, for

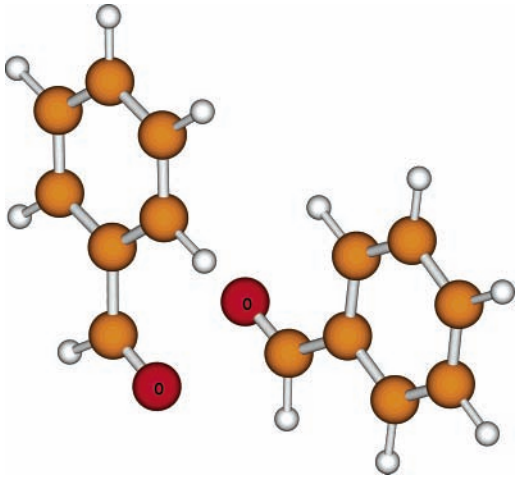

Figure 11. Structure of the benzaldehyde dimer constructed from optimized (BP86/TZP) monomers.

which local valence excitations become hidden among a multitude of CT excitations in the uncorrected calculation.

The resulting rotational strengths indeed behave as expected according to Harata's rule. Thus, they agree qualitatively with the calculations using the empirical Kirkwood-Tinoco model,[19] or the simple summation of the $(GF)_j$ factors described above: For the 0° orientation, the electric transition dipole moment of the lowest singlet excitation is (almost) parallel to the axis of the cyclodextrin, since it is perpendicular to the C−O bond and in the molecular plane (see Figure 9). Indeed, this orientation results in a positive rotational strength for the lowest singlet transition. At about 45°, the rotational strength becomes negative and reaches a minimum when the C−O bond is parallel to the cyclodextrin axis (90° orientation; note that this corresponds to the 0° orientation in ref 19, since we measure the angle of the C−O bond with respect to the cyclodextrin plane, while in that work the angle of the electric transition dipole moment with respect to the plane is used). In the latter orientation, the transition dipole moment is perpendicular to the axis of the cyclodextrin host. However, the supermolecular calculations show that the induced rotational strength is not perfectly symmetric: The signal is, for example, smaller at 0° than at 180°, but on the other hand it is larger at 60° than at 120°.

To test the performance of the frozen-density embedding, we calculated the rotational strengths for different orientations of the phenol molecule within the cyclodextrin cavity representing the latter by its frozen density. We compared two calculations, in which the density of the β-cyclodextrin was either nonpolarized or polarized by one freeze-and-thaw cycle. The nonpolarized calculations are much more efficient, since the same frozen density for the host system can be used for all different orientations of the phenol molecule. (For testing, we also carried out nonpolarized and polarized calculations in which a frozen-core was used for the oxygen- and carbon-1s orbitals (not shown). That further reduces the computational effort in the preparation step of the frozen density. It yields practically the same results as the calculation without frozen core, so that we can conclude that the frozen core approximation does not affect the embedding potential significantly.) The results are shown in Figure 10. The differences between the relaxed and nonrelaxed frozen-density schemes are almost negligible, so that we will only discuss the calculations with a relaxed frozen density (and without frozen-core approximation). The rotational strength does indeed change sign for the different orientations of the phenol molecule, but it does so in an unexpected way: At 0°, the rotational strength is close to zero. Then it goes down until it reaches a first minimum at 20°, changes sign again at about 45°, and reaches a maximum at 70°, changes sign again at ca. 95° and decreases until a second minimum is reached at 110°. Another change in sign occurs at about 130°, before the next maximum is reached at 160°. This behavior is not in line with Harata's rule, which would predict a positive rotational strength for the 0 and 180° orientations, and a negative one for the 90° orientation.

When comparing the results from the (simplified) Kirkwood-Tinoco model, the frozen-density embedding, and the supermolecular TDDFT calculation, it appears that the latter curve in Figure 10 is a superposition of a Kirkwood-Tinoco model-like symmetric curve and the curve resulting from FDE. Subtracting the embedding curve from the supermolecular one would lead to a more symmetric result; that is, it would be closer to the pure Kirkwood-Tinoco model. This can be rationalized as follows: FDE is able to describe direct effects of the host system on the density and orbitals of the guest system; that is, it shows a strong dependence on the exact position and shape of the guest molecule inside the host cavity. Because of the restricted response, however, it is not able to cover the effect of couplings with host excitations. These are, on the other hand, described by the empirical Kirkwood-Tinoco expression, whereas the only information about the guest molecule used in this empirical model is the electric transition dipole moment. Specific effects of the host on the orbitals of the embedded system are thus not included. The FDE calculations demonstrate that those are significant. The supermolecular calculation combines both effects, so that the results look like a sum of the curves obtained by FDE and the Kirkwood-Tinoco model.

6. Coupled Excitations

The phenomenon of coupling between host and guest molecule excitations evidently leads to discrepancy between FDE and the supermolecular benchmark calculations. To bring home this point, we briefly consider a case where the inadequacy of FDE stands out very sharply. There are some prototype systems consisting of several chromophores for which exciton coupling models predict the appearance of a so-called couplet.[50] A couplet can be understood as two interacting transitions of two similar chromophores that have rotational strengths of similar magnitude but opposite sign. Based on simple models employing localized wave functions[50] or on bond polarizabilities,[18,21] it is possible to estimate the splitting between two interacting transitions and their rotational strengths. Because of the interaction of the two chromophores, the positions of these transitions are not exactly the same and the CD intensities do not cancel exactly. This is demonstrated in the following for a benzaldehyde dimer as shown in Figure 11. The structure of the monomer was optimized using BP86/TZP. Since we only want to point out which type of interactions cannot be studied by frozen-density embedding, and not to investigate the properties of a real benzaldehyde dimer, we constructed an idealized dimer as a juxtaposition of a monomer with its mirror image. The mirror plane was chosen in the middle of the C═O bond (perpendicular to this bond), so that the positions of the carbonyl-C and O atoms are exchanged. Then, the reflected monomer was displaced along the *z*-axis (perpendicular to the molecular plane) by 3 Å.

Figure 12 shows the results of a supermolecular calculation for a $\pi \rightarrow \pi^*$ type transition of the benzaldehyde dimer. In this particular case, we get two transitions of different symmetry for the C_2 complex: The 8*B* transition has a strong positive rotational strength, while the 8*A* transition, which is 0.12 eV

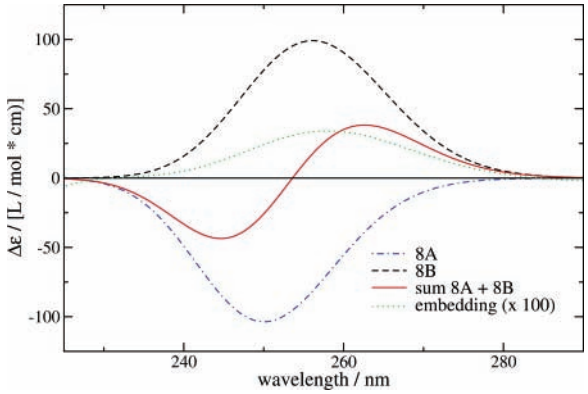

Figure 12. CD spectra of the benzaldehyde dimer shown in Figure 11 (SAOP/TZ2P). Shown are the contributions of two excitations in a supermolecular calculation as well as their sum. Additionally, the spectrum obtained in an embedding calculation is shown, which is scaled by a factor of 100.

higher in energy, shows a negative rotational strength of almost the same magnitude. The superposition results in a "couplet" with a positive part at the long-wavelength side and a negative part at the short-wavelength side.

Frozen-density embedding, as is shown in Figure 12, is not applicable if one benzaldehyde monomer is treated as a frozen system, since the response is explicitly restricted to the embedded system. This results in a very weak, positive CD signal with a maximum at 258 nm, since there is no interaction possible with a similar excitation on the other fragment (note that the signal for the embedding calculation in Figure 12 is scaled by a factor of 100). Indeed, if we calculate the CD spectrum for the second monomer keeping the first one frozen, we get exactly the same result because of the imposed C_2 symmetry of the dimer.

7. Conclusions

The examples in this work demonstrate that induced circular dichroism is a very sensitive probe of complexation and intermolecular interactions. We have shown that frozen-density embedding is very well able to predict electronic effects on circular dichroism spectra which arise because of interactions of a (nonchiral) chromophore-containing molecule with a chiral compound. This is of 3-fold advantage in comparison to supermolecular calculations on the complexes formed between such molecules: (i) The embedding calculations are computationally less demanding. This is of great importance if large host systems shall be described, which interact with a comparatively small guest molecule, or if many structures have to be evaluated, so that even moderate savings in computer time for each calculation lead to a substantial decrease in the total effort. (ii) The problem of spurious charge-transfer excitations, which can mix with the transitions under study and can hamper the interpretation, is avoided. (iii) The induced CD signals can easily be interpreted in terms of excitations localized on the embedded system. Shifts in excitation energies and changes in rotational strengths can thus be understood in terms of specific effects on the orbitals of the achiral molecule, whereas the chiral subsystem is only represented by its frozen electron density.

The embedding method is by construction not able to describe couplings to excitations that are not localized on the embedded system, which leads to a failure of FDE in cases where these effects are dominant. The reason is the same reason that is responsible for the advantages of the embedding method: the restriction of the orbital space to the embedded fragment. It should be kept in mind that *all* effective embedding methods, including QM/MM methods, necessarily have the same problem. However, as long as such couplings are not important, frozen-density embedding offers a way for an efficient description of interaction effects leading to induced circular dichroism, and it does not rely on any system-specific, empirical parametrization.

For a full interpretation of the spectra in solution arising from complex formation between chiral and achiral molecules, it is necessary to use a dynamical picture and study a representative set of snapshots from such a dynamics, including the solvent molecules. For such studies it will be advantageous if only the absorbing species, and not the chiral environment have to be treated explicitly. Although no such detailed simulation is carried out in this work, some important conclusions about specific interactions leading to induced CD effects can be drawn already from an analysis of a set of low-energy structures. This was demonstrated here for the benzoylbenzoic acid−amphetamine complex and the complex between the ferrocenecarboxylic acid-crown ether conjugate and L-leucine. Frozen-density embedding is thus a valuable method to represent complex environmental structures that induce CD activity of nonchiral compounds by specific interactions.

Acknowledgment. J. N. acknowledges funding by a Forschungsstipendium of the Deutsche Forschungsgemeinschaft (DFG).

References and Notes

(1) Allenmark, S. *Chirality* **2003**, *15*, 409−422.
(2) Takenaka, S.; Matsuura, N.; Tokura, N. *Tetrahedron Lett.* **1974**, *26*, 2325−2328.
(3) Mayer, B.; Zhang, X.; Nau, W. M.; Marconi, G. *J. Am. Chem. Soc.* **2001**, *123*, 5240−5248.
(4) Zhang, X.; Nau, W. M. *Angew. Chem., Int. Ed.* **2000**, *39*, 544−547.
(5) Kamiya, M.; Mitsuhashi, S.; Makino, M.; Yoshioka, H. *J. Phys. Chem.* **1992**, *96*, 95−99.
(6) Najiwara, S.; Kawamura, M.; Yamaguchi, H. *Helv. Chim. Acta* **2000**, *83*, 2783−2786.
(7) Kawamura, M.; Higashi, M. *Helv. Chim. Acta* **2003**, *86*, 2342−2348.
(8) Harata, K.; Uedaira, H. *Bull. Chem. Soc. Jpn* **1975**, *48*, 375−378.
(9) Kodaka, M. *J. Phys. Chem. A* **1998**, *102*, 8101−8103.
(10) Murphy, R. S.; Barros, T. C.; Barnes, J.; Mayer, B.; Marconi, G.; Bohne, C. *J. Phys. Chem. A* **1999**, *103*, 137−146.
(11) Connors, K. A. *Chem. Rev.* **1997**, *97*, 1325−1357.
(12) Rekharsky, M. V.; Inoue, Y. *Chem. Rev.* **1998**, *98*, 1875−1917.
(13) Tokura, N.; Nagai, T.; Takenaka, S.; Oshima, T. *J. Chem. Soc., Perkin Trans. 2* **1974**, 337−342.
(14) Takenaka, S.; Kondo, K.; Tokura, N. *J. Chem. Soc., Perkin Trans. 2* **1975**, 1520−1524.
(15) Tsukube, H.; Fukui, H.; Shinoda, S. *Tetrahedron Lett.* **2001**, *42*, 7583−7585.
(16) Lipkowitz, K. B. *Chem. Rev.* **1998**, *98*, 1829−1873.
(17) Kirkwood, J. P. *J. Chem. Phys.* **1937**, *5*, 479−491.
(18) Tinoco, I. *Adv. Chem. Phys.* **1962**, *4*, 113−160.
(19) Shimizu, H.; Kaito, A.; Hatano, M. *Bull. Chem. Soc. Jpn.* **1979**, *52*, 2678−2684.
(20) Shimizu, H.; Kaito, A.; Hatano, M. *Bull. Chem. Soc. Jpn.* **1981**, *54*, 513−519.
(21) Kodaka, M. *J. Phys. Chem.* **1991**, *95*, 2110−2112.
(22) Kodaka, M. *J. Am. Chem. Soc.* **1993**, *115*, 3702−3705.
(23) Dreuw, A.; Weisman, J. L.; Head-Gordon, M. *J. Chem. Phys.* **2003**, *119*, 2943−2946.
(24) Tawada, Y.; Tsuneda, T.; Yanagisawa, S.; Yanai, T.; Hirao, K. *J. Chem. Phys.* **2004**, *120*, 8425−8433.
(25) Gritsenko, O.; Baerends, E. J. *J. Chem. Phys.* **2004**, *121*, 655−660.
(26) Neugebauer, J.; Louwerse, M. J.; Baerends, E. J.; Wesolowski, T. A. *J. Chem. Phys.* **2005**, *122*, 094115.
(27) Neugebauer, J.; Jacob, C. R.; Wesolowski, T. A.; Baerends, E. J. *J. Phys. Chem. A* **2005**, *109*, 7805−7814.
(28) Wesolowski, T. A.; Warshel, A. *J. Phys. Chem.* **1993**, *97*, 8050.
(29) Wesolowski, T. A.; Weber, J. *Int. J. Quantum Chem.* **1997**, *61*, 303.

(30) Casida, M. E.; Wesolowski, T. A. *Int. J. Quantum Chem.* **2004**, *96*, 577−588.
(31) Wesolowski, T. A. *J. Am. Chem. Soc.* **2004**, *126*, 11444−11445.
(32) Schipper, P. R. T.; Gritsenko, O. V.; van Gisbergen, S. J. A.; Baerends, E. J. *J. Chem. Phys.* **2000**, *112*, 1344−1352.
(33) Gritsenko, O. V.; Schipper, P. R. T.; Baerends, E. J. *Chem. Phys. Lett.* **1999**, *302*, 199−207.
(34) Gritsenko, O. V.; Schipper, P. R. T.; Baerends, E. J. *Int. J. Quantum Chem.* **2000**, *76*, 407−419.
(35) Becke, A. D. *Phys. Rev. A* **1988**, *38*, 3098−3100.
(36) Perdew, J. P. In *Electronic Structure of Solids*; Ziesche, P., Eschrig, H., Eds.; Akademie Verlag: Berlin, 1991.
(37) Jacob, C. R.; Wesolowski, T. A.; Visscher, L. *J. Chem. Phys.* **2005**, *123*, 174104.
(38) Theoretical Chemistry, Vrije Universiteit Amsterdam. Amsterdam Density Functional Program. URL: http://www.scm.com.
(39) te Velde, G.; Bickelhaupt, F. M.; Baerends, E. J.; Fonseca Guerra, C.; van Gisbergen, S. J. A.; Snijders, J. G.; Ziegler, T. *J. Comput. Chem.* **2001**, *22*, 931−967.
(40) Perdew, J. P. *Phys. Rev. B* **1986**, *33*, 8822−8824.
(41) Autschbach, J.; Ziegler, T. *J. Chem. Phys.* **2002**, *116*, 891−896.
(42) Autschbach, J.; Ziegler, T.; van Gisbergen, S. J. A.; Baerends, E. J. *J. Chem. Phys.* **2002**, *116*, 6930−6940.
(43) Autschbach, J.; Ziegler, T.; Patchkovskii, S.; van Gisbergen, S. J. A.; Baerends, E. J. *J. Chem. Phys.* **2002**, *117*, 581−592.
(44) van Gisbergen, S. J. A.; Snijders, J. G.; Baerends, E. J. *Comput. Phys. Commun.* **1999**, *118*, 119−138.
(45) Schaftenaar, G. *Molden3.7: a pre- and postprocessing program of molecular and electronic structure;* CMBI: The Netherlands, 2001.
(46) Humphrey, W.; Dalke, A.; Schulten, K. *J. Mol. Graphics* **1996**, *14.1*, 33−38.
(47) Nicu, V. P.; Neugebauer, J.; Baerends, E. J. Unpublished work.
(48) Neugebauer, J.; Baerends, E. J.; Nooijen, M.; Autschbach, J. *J. Chem. Phys.* **2005**, *122*, 234305.
(49) Neugebauer, J.; Gritsenko, O.; Baerends, E. J. *J. Chem. Phys.* **2006**, *124*, 214102.
(50) Klessinger, M.; Michl, J. *Lichtabsorption und Photochemie organischer Moleküle*; Verlag Chemie: Weinheim, Germany, 1989.